Title

Using a system's equilibrium behavior to reduce its energy dissipation in nonequilibrium processes

Journal

Proceedings of the National Academy of Sciences of the United States of America, 116(13)

ISSN

0027-8424

Authors

Tafoya, Sara
Large, Steven J
Liu, Shixin
et al.

Publication Date

2019-03-26

DOI

10.1073/pnas.1817778116

Peer reviewed

Using a system's equilibrium behavior to reduce its energy dissipation in nonequilibrium processes

Sara Tafoya[a,b,c,1,2], Steven J. Large[d,1], Shixin Liu[e], Carlos Bustamante[a,b,c,f,g,h,i,j,3], and David A. Sivak[d,3]

[a]Jason L. Choy Laboratory of Single Molecule Biophysics, University of California, Berkeley, CA 94720; [b]Howard Hughes Medical Institute, University of California, Berkeley, CA 94720; [c]Biophysics Graduate Group, University of California, Berkeley, CA 94720; [d]Department of Physics, Simon Fraser University, Burnaby, BC V5A 1S6, Canada; [e]Laboratory of Nanoscale Biophysics and Biochemistry, The Rockefeller University, New York, NY 10065; [f]Department of Molecular and Cell Biology, University of California, Berkeley, CA 94720; [g]Department of Physics, University of California, Berkeley, CA 94720; [h]Department of Chemistry, University of California, Berkeley, CA 94720; [i]California Institute for Quantitative Biosciences, University of California, Berkeley, CA 94720; and [j]Kavli Energy Nanoscience Institute, University of California, Berkeley, CA 94720

Edited by Attila Szabo, NIH, Bethesda, MD, and approved February 12, 2019 (received for review October 21, 2018)

Cells must operate far from equilibrium, utilizing and dissipating energy continuously to maintain their organization and to avoid stasis and death. However, they must also avoid unnecessary waste of energy. Recent studies have revealed that molecular machines are extremely efficient thermodynamically compared with their macroscopic counterparts. However, the principles governing the efficient out-of-equilibrium operation of molecular machines remain a mystery. A theoretical framework has been recently formulated in which a generalized friction coefficient quantifies the energetic efficiency in nonequilibrium processes. Moreover, it posits that, to minimize energy dissipation, external control should drive the system along the reaction coordinate with a speed inversely proportional to the square root of that friction coefficient. Here, we demonstrate the utility of this theory for designing and understanding energetically efficient nonequilibrium processes through the unfolding and folding of single DNA hairpins.

single molecule | nonequilibrium | dissipation | DNA hairpins | energetic efficiency

Reversible heat engines operating infinitely slowly according to the Carnot cycle do not dissipate energy; their energetic efficiency is limited only by the entropy increase of the surroundings associated with the transfer of heat from a hot to a cold reservoir. In contrast, for engines operating irreversibly, the extra nonequilibrium energy cost associated with carrying out a process at a finite rate further reduces their efficiency (1). This is the case of biological machines (2) that must operate under signaling, transport, and cell cycle time constraints. For instance, F_oF_1-ATP synthase, the primary machine responsible for ATP synthesis, can rotate up to ∼350 revolutions per second (3); the bacteriophage φ29 packaging motor internalizes the 19.3-kbp viral genome into a small capsid at rates of 100 bp/s—faster than the relaxation rate of the confined DNA (4); and during sporulation, the *Bacillus subtilis* DNA translocase, SpoIIIE, transfers two-thirds of its 4.2×10^6-bp genome between mother cell and prespore in only 15 min (i.e., at a transfer rate of nearly 4,000 bp/s) (5). The finite time operations of these machines necessarily involve energy dissipation—often in the form of extra work—and it is of great interest to understand how they attain their large (over 70%) energetic efficiencies (6, 7).

Recently, a generalized friction coefficient—which can be obtained from equilibrium measurements—was shown to be the parameter that governs the near-equilibrium energy dissipation during a finite rate process (8). Here, we demonstrate experimentally the utility of this theoretical framework for designing energetically efficient nonequilibrium processes and propose that similar operation protocols may underlie the high efficiency observed in molecular machines. To this end, we subject single DNA hairpins to mechanical unfolding and refolding using protocols dictated by this theory; we show that these protocols systematically and significantly reduce energy dissipation during the process. DNA hairpins are ideally suited for this test, as the magnitude of the friction coefficient can be tuned by changing the molecule's length, the free energy difference, the free energy barrier, and the transition rates between its folded and unfolded states (9).

According to this near-equilibrium linear response theory, the excess power dissipated by a system taken from an initial to a final state by varying a control parameter λ according to a protocol (time schedule) Λ is proportional to a generalized friction coefficient ζ (8):

$$\langle \mathcal{P}_{\mathrm{ex}}(t) \rangle \approx \zeta(\lambda) \left(\frac{d\lambda}{dt} \right)^2 . \qquad [1]$$

ζ generalizes the standard macroscopic friction coefficient in a viscous medium (10) to describe resistance to rapid changes of any (not necessarily spatial) control parameter. Importantly, the theory shows that ζ can be computed from the fluctuations $\delta F(t) = F(t) - \langle F \rangle$ of the force $F(t)$ via the time integral of the force autocorrelation function $\langle \delta F(0) \delta F(t) \rangle_\lambda$,

$$\zeta(\lambda) = \beta \int_0^\infty \langle \delta F(0) \delta F(t) \rangle_\lambda \, dt, \qquad [2]$$

which can be decomposed into

Significance

Biomolecular machines implement many vital activities in cells and must operate quickly and in functional directions, requiring energy dissipation. Recent experiments reveal that some evolved machines are quite energetically efficient, engendering interest in design principles that achieve such high efficiency. Recent theory predicts how to use equilibrium measurements (in the absence of driving) to design ways to drive a system to minimize energy dissipation. Here, we experimentally demonstrate the utility of this theory for designing efficient driving processes ("protocols") by rapidly unfolding and folding single DNA hairpins. We show that such designed protocols systematically and significantly reduce energy dissipation over large variations of driving speed and DNA hairpin friction. Similar protocols may underlie the high efficiency observed in molecular machines.

Author contributions: S.T., S.J.L., S.L., C.B., and D.A.S. designed research; S.T. performed research; S.J.L. and D.A.S. analyzed data; and S.T., S.J.L., S.L., C.B., and D.A.S. wrote the paper.

The authors declare no conflict of interest.

This article is a PNAS Direct Submission.

[1]S.T. and S.J.L. contributed equally to this work.

[2]Present address: Scientific Application Development Group, Lumicks, Cambridge, MA 02139.

[3]To whom correspondence may be addressed. Email: carlosb@berkeley.edu or dsivak@sfu.ca.

This article contains supporting information online at www.pnas.org/lookup/suppl/doi:10.1073/pnas.1817778116/-/DCSupplemental.

Published online March 13, 2019.

$$\zeta(\lambda) = \beta\langle \delta F^2 \rangle_\lambda \, \tau_{\text{relax}}(\lambda), \quad [3]$$

the product of the force variance $\langle \delta F^2 \rangle_\lambda$ and the force relaxation time

$$\tau_{\text{relax}}(\lambda) = \int_0^\infty \frac{\langle \delta F(0) \delta F(t) \rangle_\lambda}{\langle \delta F^2 \rangle_\lambda} \, dt. \quad [4]$$

Here, $\langle \ldots \rangle$ denotes a nonequilibrium average over system response to a given protocol, whereas $\langle \ldots \rangle_\lambda$ denotes an equilibrium average over system fluctuations at fixed control parameter λ. Notice that this framework makes no assumptions about the hairpin dynamics being Markovian and that the force autocorrelation function is well defined regardless of whether the dynamics is Markovian (11).

It can be shown (12) that, near equilibrium, the driving protocol that minimizes the dissipation for a given total duration, $\lambda(t)_{\text{designed}}$, must proceed with a velocity proportional to the inverse square root of the local friction coefficient $\zeta(\lambda)$, $d\lambda(t)_{\text{designed}}/dt \propto \zeta(\lambda)^{-1/2}$. The proportionality is fixed by the total duration of the protocol, and therefore, changing it corresponds to a global rescaling of all velocities. Other approaches to minimizing work (13, 14) require detailed knowledge of both the system's equilibrium energy landscape and nonequilibrium dynamics and thus, are experimentally challenging.

To obtain the generalized friction coefficient of the DNA hairpin, we monitored the equilibrium force fluctuations of molecules tethered between two optical traps at various fixed trap separations, X. For very small or very large trap separations, the force fluctuates around a single mean value corresponding to the folded or unfolded conformation, respectively (Fig. 1*A*); for intermediate trap separations, the force fluctuates between two different values, reflecting the hopping dynamics of the DNA hairpin sampling the folded and unfolded conformations (Fig. 1*A*). For each separation X, we calculated the force autocorrelation function, $\langle \delta F(0) \delta F(t) \rangle_X$ (Fig. 1*C*); as expected, in the hopping regime, the force variance is larger, and fluctuations decay more slowly than when an extreme trap separation holds the DNA hairpin in a single conformation.

Next, we calculated the force variance (Fig. 1*D*) and the force relaxation time (Fig. 1*E*) from the force autocorrelation function. The force variance peaks at an intermediate trap separation, $X_{1/2}$, where the hairpin spends roughly equal time between the folded and unfolded conformations. Likewise, the force relaxation time peaks at $X_{1/2}$, reflecting that, to equilibrate, the hairpin must relax across the barrier separating the folded and unfolded states. At room temperature, a 1-μm bead experiencing Stokes drag (with friction $\gamma = \pi\eta R$ for water viscosity η and bead radius R) in water and confined by a $k = 0.25$-pN/nm optical trap has a relaxation time $\gamma/k \sim 30$ μs (15), orders of magnitude below the minimum observed relaxation time of the entire construct—indicating that the beads do not significantly impact the relaxation times observed in the experiments, typically in the low milliseconds. Moreover, the generalized friction coefficient—the product of force variance and force relaxation time (Eq. 3)—also peaks at $X_{1/2}$ (Fig. 1*F*).

As mentioned above, the theory predicts that (near equilibrium) the minimum dissipation protocol proceeds with a pulling speed—or velocity of the steering trap—that scales as the inverse square root of the friction coefficient (8): pulling fast at extreme separations, where the friction coefficient is small, and slow around $X_{1/2}$, where friction peaks. Intuitively, a slow velocity near $X_{1/2}$ provides more time for thermal fluctuations to induce the unfolding or folding of the DNA hairpin without additional work input and therefore, decreases the work required to drive the DNA hairpin between conformations (12). To ease its

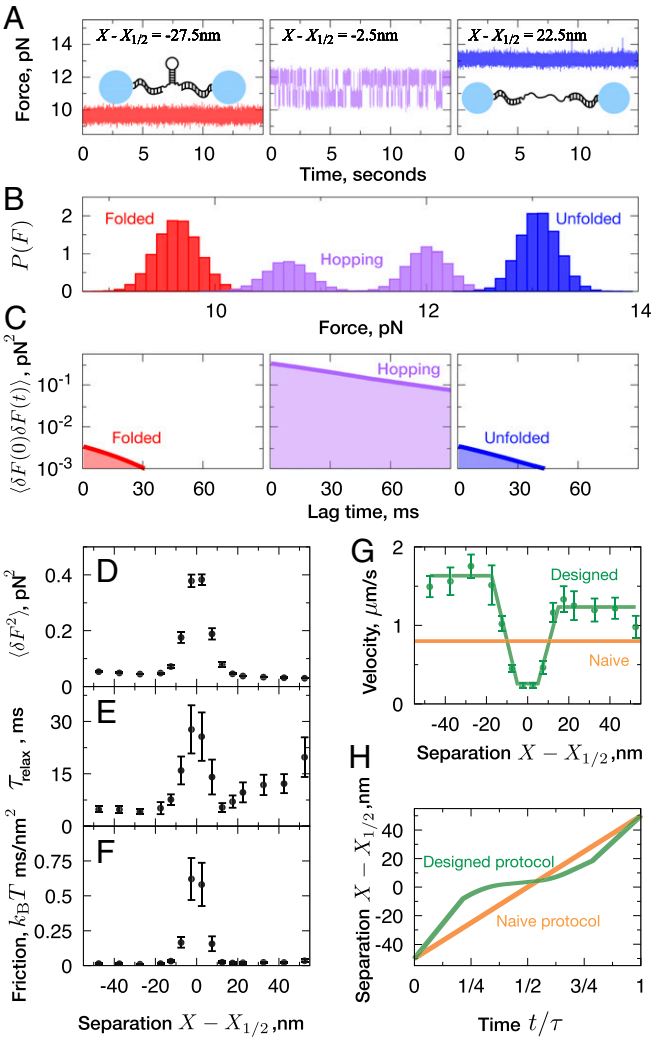

Fig. 1. Equilibrium sampling reveals that the friction coefficient peaks strongly at the hopping regime. (*A*) Sample force traces as a function of time for folded hairpin (*Left*; red), hopping hairpin (*Center*; purple), and unfolded hairpin (*Right*; blue). (*B*) Equilibrium force distributions and (*C*) force correlation as a function of lag time for corresponding fixed optical trap separations. (*D*) Force variance $\langle \delta F^2 \rangle_x$, (*E*) force relaxation time $\tau_{\text{relax}}(X)$, and their product (*F*) the generalized friction coefficient $\zeta(X)$ as a function of fixed optical trap separation. (*G*) For a 0.13-s protocol duration, the designed velocity $dX/dt \propto \zeta^{-1/2}$ (green points) with best-fit model (green curve) minimizes Akaike information criterion (30) compared with naive velocity (orange line). (*H*) Designed and naive velocities scale inversely with protocol duration τ, and designed (green) and naive (yellow) protocols are plotted as functions of t/τ.

implementation, the designed protocol that minimizes dissipation was approximated by a trap velocity profile with a simple piecewise-constant acceleration (Fig. 1*G*). The resulting designed protocols (Fig. 1*H*) differ substantially from naive protocols that proceed at constant velocity and that are completed in the same elapsed time. In particular, instantaneous driving velocities varied by a factor of approximately six within a given designed protocol.

Next, we measured force as a function of trap separation during designed and naive protocols with total durations ranging from 3.7 to 0.13 s. These force separation curves of naive and designed protocols display significant differences in the force at which the DNA hairpins unfold/refold (Fig. 2*A*). Fig. 2*B* shows the distributions of unfolding force differences, $F^{\text{U}}_{\text{naive}} - F^{\text{U}}_{\text{designed}}$,

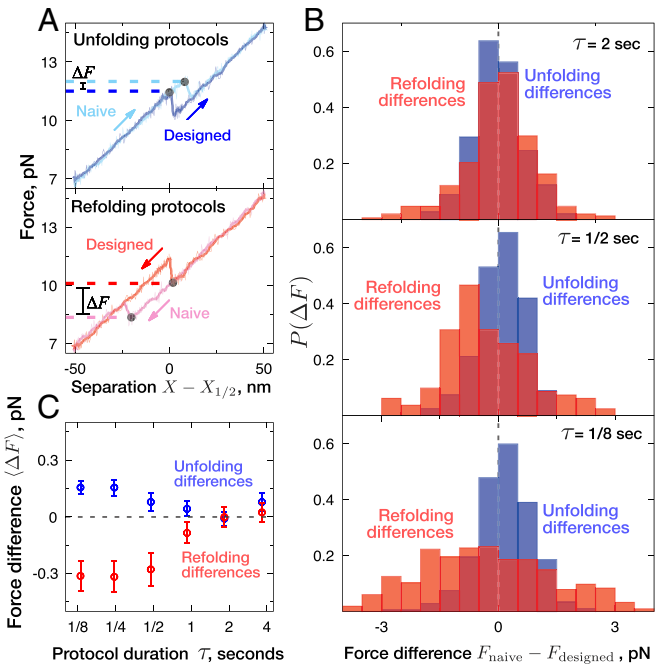

Fig. 2. Designed protocols consistently unfold at lower force and refold at higher force. (*A*) Example force separation curves from a sample molecule for protocol duration $\tau = 0.13$ s, highlighting the unfolding (*Upper*) and refolding (*Lower*) events (black dots) and the corresponding forces (dashed lines) for designed (dark blue and dark red) and naive (light blue and pink) protocols. The raw data (thin lines) are Savitsky–Golay filtered to obtain a smoothed force separation curve (thick lines). (*B*) Distributions of differences $F_{\text{naive}} - F_{\text{designed}}$ between naive and designed unfolding (blue) and refolding (red) forces. (*C*) Mean and SE for unfolding and refolding force differences as a function of protocol duration. On average, the designed protocol unfolds at a lower force and refolds as a higher force than the corresponding naive protocol.

and refolding force differences, $F^{\text{R}}_{\text{naive}} - F^{\text{R}}_{\text{designed}}$, obtained for three different protocol durations. As predicted by theory, on average, the DNA hairpin unfolded at lower forces and refolded at higher forces during the designed protocols than during the naive protocols, and the magnitude of the mean force difference is greater for faster protocols (Fig. 2*C*). These results imply that the designed protocols display lower hysteresis than naive, a trend that is more prominent in faster protocols where the system is driven farther from equilibrium.

Analogous to Fig. 2*A*, Fig. 3*A* depicts the cycle work for a typical realization of an unfolding/refolding cycle. According to Eq. 1, when driving a system at a constant velocity, more work is dissipated at trap separations where the friction coefficient is larger. Consistently, the constant velocity protocols produce higher dissipation around $X_{1/2}$ for all durations (Fig. 3*B*); by contrast, designed protocols show a substantially flatter dissipation profile across different trap separations (Fig. 3*B*), and overall, they induce consistently less dissipation during an unfolding–refolding cycle than naive protocols (Fig. 3 *C* and *D*). Within the linear response regime, the mean dissipated work equals one-half the work variance; *SI Appendix*, Fig. S3 shows that, in our experiments, this relation holds for slower protocols. The mean and variance of the distribution of cycle work $(W^{\text{U}} + W^{\text{R}})$ for both protocol types are higher at shorter protocol duration (Fig. 3*C*), consistent with higher hysteresis. Finally, the faster designed protocols save even more work relative to their naive counterparts than slower protocols do (Fig. 3*D*). Molecular motors can operate as much as 100 times faster than our fastest protocols (16); therefore, the work differences are expected to be substantially larger for such rapid protocols.

The data presented here correspond to a DNA hairpin that allowed relatively rapid folded–unfolded equilibration such that transitions to the folded or unfolded conformations occurred even for 0.13-s protocols. This feature allowed us to interrogate the hairpin's nonequilibrium response over a broad range of protocol durations. In *SI Appendix*, we show that these results also hold for a different DNA hairpin sequence with significantly (~100 times) slower equilibration.

In summary, we have sampled the equilibrium force fluctuations in DNA hairpins, displaying the dynamics of a two-state system (Fig. 1). We showed that the generalized friction coefficient—determined from such equilibrium fluctuations—can be used to design driving schedules (Fig. 1*G*) that significantly

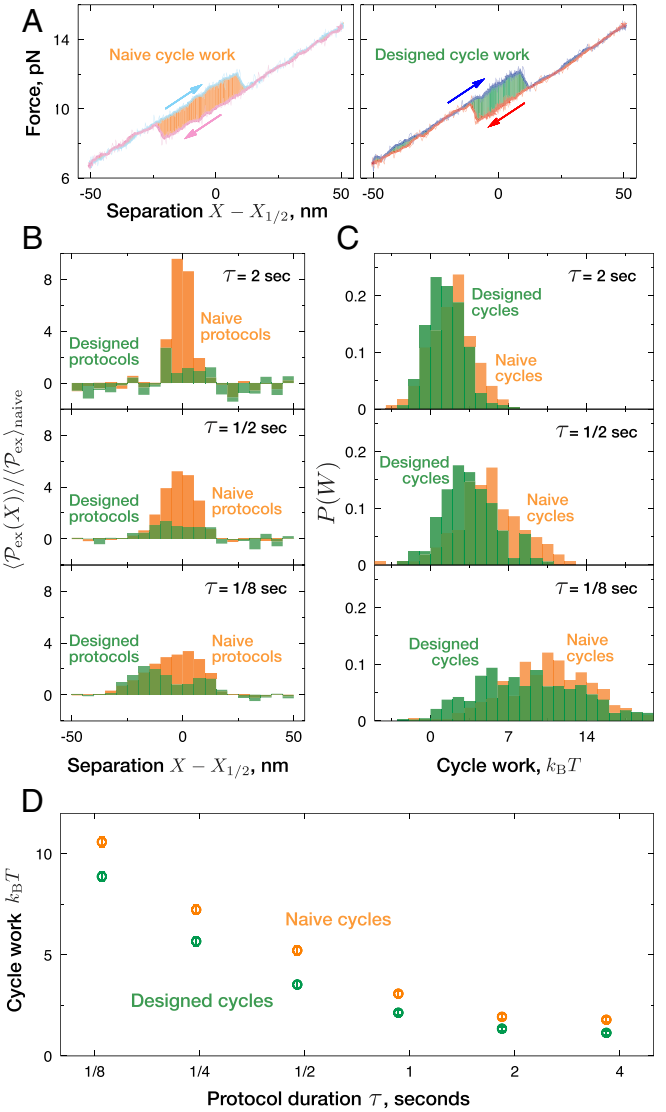

Fig. 3. Designed protocols consistently require less work than corresponding naive protocols. (*A*) Example force separation curves showing the cycle work $W^{\text{U}} + W^{\text{R}}$ for naive (*Left*; orange) and designed (*Right*; green) protocols. The raw force separation curve (thin) is smoothed by a Savitsky–Golay filter (thick). (*B*) Excess power $\langle \mathcal{P}_{\text{ex}}(X) \rangle / \langle \mathcal{P}_{\text{ex}} \rangle_{\text{naive}}$ normalized by average naive excess power as a function of trap separation for naive (yellow) and designed (green) protocols. (*C*) Distributions of cycle work $W^{\text{U}} + W^{\text{R}}$ for naive (yellow) and designed (green) protocols for protocols ranging from slow (*Top*) to fast (*Middle* and *Bottom*). (*D*) Mean cycle work $\langle W^{\text{U}} + W^{\text{R}} \rangle$ during naive (green) and designed (orange) protocols as a function of protocol duration.

reduce the excess work dissipated compared with constant velocity schedules (naive protocols) completed in the same total time (Fig. 3*D*). This result held for protocol durations that vary by a factor of ∼30 (Fig. 3*D*), even when driven far from equilibrium (dissipating up to ∼10 k_BT, which greatly exceeds the ∼1-k_BT energy fluctuations at equilibrium). These observations indicate that this near-equilibrium theory is still able to reduce dissipation even beyond the regime of the theory's strict validity.

This experiment represents the design and implementation of a single-molecule protocol that systematically reduces the nonequilibrium energy dissipation in a process constrained to a finite duration.

These results have immediate applications in the streamlining of single-molecule experiments and steered molecular dynamics simulations (17). For instance, when using the Jarzynski equality or Crooks fluctuation theorem to infer the free energy difference in a given process (such as protein unfolding), the farther the system is from equilibrium during experiment or simulation, the slower the rate of convergence and accuracy of the free energy estimator, which depends inversely on the energy dissipated (18). Therefore, by sampling the equilibrium fluctuations of a biomolecular process, it should be possible to estimate the generalized friction coefficient across the control parameter landscape; next, it would be possible to craft nonequilibrium protocols that dissipate significantly less energy, thereby speeding up the convergence and increasing the accuracy of any given free energy estimator.

There are tantalizing hints of molecular machines conserving energy while operating out of equilibrium (4, 19): the φ29 DNA packaging motor is more likely to slow down and pause at high packaging fractions, where the storing of additional DNA involves significantly higher dissipation, and translating ribosomes facing RNA hairpins—that impose a large barrier to translation—change "gear," operating slower while crossing the barrier (20). Based on the theoretical framework presented here, both cases can be seen as examples in which the molecular machines implement driving protocols that proceed slower where the friction coefficient is higher, thereby reducing dissipation and increasing their efficiency. We hypothesize that a molecular biophysical system can waste less energy through naturally evolved dynamics that is rationalizable in terms of the generalized friction coefficient; specifically, such molecular motors may have evolved to slow down their operation in regions of their control parameter space corresponding to high values of the friction coefficient as a way to harness fluctuations from the thermal bath, thus improving their operation efficiency.

The agreement of theory (8) and our experiments suggests extensions to more complex contexts. In particular, we conjecture that molecular machines may have evolved to slow down in regions of large friction and speed up in regions of small friction. The rotary motor F_1-ATP synthase is known to be a remarkably efficient machine (21), where the F_o subunit–powered by proton flow down a concentration gradient–forces rotation of the γ-subunit, a molecular crankshaft that drives synthesis of ATP by F_1 (6). After attaching a magnetic bead to the crankshaft of F_1 (22), one could–analogous to the procedure described in this study–use a magnetic tweezers instrument to hold the bead at various angles so as to extract the equilibrium torque fluctuations of the rotary crankshaft, from which one could extract the friction coefficient at each position (in this experiment, the angle corresponds to the control parameter for driving F_1 in analogy to the trap separation for driving the unfolding of the DNA hairpin). One could then estimate the minimum dissipation protocol and determine the ratio of energy input (work done to rotate the crankshaft) to energy output (ATP molecules synthesized) (22, 23) for designed and naive protocols. These ratios quantify the energetic efficiency with which the respective protocols induce F_1 to synthesize ATP, and their difference determines the energetic savings.

We have seen here that the linear response theory provides a useful qualitative guide to design protocols that systematically require less work than naive ones. Moreover, since this theoretical framework naturally generalizes to stochastic protocols (24), future experiments could be designed to more closely match autonomous machines driven by fluctuating forces. Insights from the experiments designed with this framework should provide a deeper understanding of the nonequilibrium energetic efficiency of biomolecular machines and ultimately, guide the operation of efficient synthetic nanomachines.

Materials and Methods

Basic Optical Trap Setup. High-resolution force separation measurements were conducted on a dual-trap instrument using a solid-state 1,064-nm laser as described previously (25). Traps were calibrated as previously described (26). DNA tethers were formed between a 0.90-μm-diameter streptavidin-coated bead and a 1-μm-diameter antidigoxigenin-coated bead (Spherotech) held in separate optical traps. An oxygen scavenging system [100 μg mL^{-1} glucose oxidase, 5 mg mL^{-1} dextrose (Sigma-Aldrich), 20 μg mL^{-1} catalase (Calbiochem)] was included in the buffer to prevent the formation of reactive singlet oxygen, thus increasing the lifetime of the DNA tethers.

DNA Molecules. Hairpin DNA sequences were selected to display hopping dynamics such that determining $X_{1/2}$ was accessible experimentally—very fast hopping dynamics were difficult to distinguish from noise, and very slow dynamics required long periods of data acquisition and laser exposure before pulling experiments. Minimizing laser exposure avoids molecule photodamage. All data in *SI Appendix* are from sequence 1, GAGTCCTGGATCCTGTTTTTTTTCAGGATCCAGGACTC, which was previously characterized and exhibited appropriate hopping dynamics ($t_{1/2} \approx 0.24$ s) (9). All data in the text are from sequence 2, TACCTGATCAGGTGCTTTTTTTTGCACCTGATCAGGTA, the result of modifying sequence 1 to increase GC content at the loop neck. This change in sequence is expected to facilitate nucleation of the native conformation and to avoid molecule misfolding (27).

Bead size variation, small differences in chemical attachments, and nonspecific interactions with the bead surface can lead to molecule to molecule variation. We minimized the contribution of trap distance variation by subtracting the value of $X_{1/2}$ in all cases. However, other unaccounted sources, such as error in stiffness calibration (most commercially available beads have root-mean-square variations in radius of 3–6%, and therefore, the error in stiffness calibration is ∼4%, assuming a 4% error in reported bead size using individual calibration measurements for each bead pair) and natural variation in the molecules' persistence length [the SD in persistence length measurement can be as high as ∼17% (28)], also contributed to molecule to molecule variation in unfolding/refolding trajectories.

Equilibrium Sampling. Each of 20 molecules is initially probed to find $X_{1/2}$: the distance between the traps is increased gradually until the residence time at folded and unfolded conformations is ∼50%. On identification of $X_{1/2}$, a systematic error of −2.5 nm was introduced in the absolute distance between the two traps. This error was introduced as a small difference of a few millivolts between the instruction given by the computer and the actual analog number instructed to the steering mirror of the trap. This problem is not present when measuring changes in separation, because in calculating relative distances, the offset is canceled. We theoretically estimated the error introduced in a designed protocol offset by this amount and found that such error should lead to a cycle work overestimate of ∼6%.

For each molecule, each separation is sampled for 30 s in order from smallest ($X_{1/2}$ − 50 nm) to largest separation ($X_{1/2}$ + 50 nm) at 10-nm spacing far from $X_{1/2}$ and 5-nm spacing near $X_{1/2}$ to more precisely resolve the friction variation at the hopping regime. Changes in separation are instructed to be performed instantaneously but are limited by the response of the mirror controlling the steering trap (∼2 ms).

Equilibrium force fluctuations at each of several fixed separations were measured independently in each of 20 different molecules. From these fluctuations, the generalized friction coefficient was estimated using Eq. **2**. At each separation, we jackknife resampled from the set of 20 friction estimates to calculate the mean generalized friction and SE (29).

We fit several piecewise-constant acceleration profiles of protocol velocity to the minimum dissipation one ($d\lambda_{\text{designed}}/dt \propto [\zeta(\lambda)]^{-1/2}$) predicted from the empirically determined generalized friction $\zeta(\lambda)$. Each model velocity profile has constant velocity (zero acceleration) far away from $X_{1/2}$ and in the immediate vicinity of $X_{1/2}$. Constant acceleration regions interpolate

between these constant velocity regions. The model parameters are the region boundaries and the constant velocities. Different model velocity profiles impose different symmetries, such as inversion symmetry about $X_{1/2}$, thus reducing the number of free parameters. We used the velocity profile (Fig. 1) that minimized the Akaike Information Criterion (30), a measure of a model's balance between accuracy and complexity.

Naive and Designed Protocols. We estimate the work W during a trajectory of forces F_i and separations X_i at n discrete time points by numerical integration:

$$W = \sum_{i=2}^{n} \frac{F_i + F_{i-1}}{2} (X_i - X_{i-1}). \quad [5]$$

There are 14, 9, 8, 8, 10, and 9 separate molecules sampled with 888 (444), 590 (295), 396 (198), 590 (295), 592 (296), and 472 (236) individual realizations (full cycles) of protocols for durations of 0.13, 0.24, 0.48, 0.93, 1.8, and 3.7 s, respectively. The cycle work (hysteresis) $W_{\text{cycle}} = W^{\text{U}} + W^{\text{R}} = W^{\text{U}}_{\text{ex}} + W^{\text{R}}_{\text{ex}}$ sums the forward and reverse realizations of a protocol at a given speed within protocols taken from the same molecule. By canceling the equilibrium free energy changes during the unfolding and refolding trajectories, this gives the sum of the excess work in each direction.

We investigate six different protocol durations ranging from 0.13 to 3.7 s. For each protocol duration, we calculate the work along ∼1,200 individual realizations, ∼300 of each of the four protocol types: designed or naive and unfolding or refolding.

To estimate the unfolding (refolding) force in a given force separation curve, we first smooth the force trace using a second-order Savitsky–Golay filter with window width of ∼0.4 ms. We report the unfolding (refolding) force as the maximum (minimum) force before the final unfolding (refolding) event takes place. We control for intermolecular variation by analyzing the difference between unfolding/refolding forces along naive and designed protocols for a given molecule instead of raw unfolding/refolding forces.

The excess power in a protocol interval (Fig. 3*B*) is calculated by adding the total unfolding work in an interval ΔX to the total refolding work in the same interval and dividing by the time taken for the protocol to traverse that separation interval. Finally, the power in each interval is normalized by the average naive excess power (averaged over the entire protocol).

ACKNOWLEDGMENTS. We thank Nancy Forde, John Bechhoefer, Aidan Brown, and Kamdin Mirsanaye (Simon Fraser University); Michael Woodside (University of Alberta); and Ronen Gabizon and Antony Lee (University of California, Berkeley) for useful discussions. This work is supported in part by the Nanomachines program (KC1203) funded by the office of Basic Energy Sciences of the US Department of Energy [contract no. DE-AC02-05CH11231 (to C.B.)]; the University of California Mexus graduate fellowship (to S.T.); Natural Sciences and Engineering Research Council of Canada (NSERC) Canada Graduate Scholarships-Master's and Alexander Graham Bell Canada Graduate Scholarships-Doctoral (to S.J.L.); the Howard Hughes Medical Institute (C.B.); an NSERC Discovery Grant (to D.A.S.); the Faculty of Science, Simon Fraser University through President's Research Startup Grant (to D.A.S.); and a Tier-II Canada Research Chair (D.A.S.).

1. Callen HB (1985) *Thermodynamics and an Introduction to Thermostatistics* (Wiley, New York).
2. Howard J (2001) *Mechanics of Motor Proteins and the Cytoskeleton* (Sinauer Associates, Sunderland, MA).
3. Ueno H, Suzuki T, Kinosita K, Jr, Yoshida M (2005) ATP-driven stepwise rotation of FoF1-ATP synthase. *Proc Natl Acad Sci USA* 102:1333–1338.
4. Berndsen ZT, Keller N, Grimes S, Jardine PJ, Smith DE (2014) Nonequilibrium dynamics and ultraslow relaxation of confined DNA during viral packaging. *Proc Natl Acad Sci USA* 111:8345–8350.
5. Besprozvannaya M, Pivorunas VL, Feldman Z, Burton BM (2013) SpoIIIE protein achieves directional DNA translocation through allosteric regulation of ATPase activity by an accessory domain. *J Biol Chem* 288:28962–28974.
6. Kinosita K, Jr, Yasuda R, Noji H, Adachi K (2000) A rotary molecular motor that can work at near 100% efficiency. *Philos Trans R Soc Lond B Biol Sci* 355:473–489.
7. Cross RA (1997) Molecular motors: The natural economy of kinesin. *Curr Biol* 7: R631–R633.
8. Sivak DA, Crooks GE (2012) Thermodynamic metrics and optimal paths. *Phys Rev Lett* 108:190602.
9. Woodside MT, et al. (2006) Nanomechanical measurements of the sequence-dependent folding landscapes of single nucleic acid hairpins. *Proc Natl Acad Sci USA* 103:6190–6195.
10. Kirkwood JG (1946) The statistical mechanical theory of transport processes I. general theory. *J Chem Phys* 14:180–201.
11. Hanggi P (1978) Correlation functions and master equations of generalized (non-Markovian) Langevin equations. *Z Phys B* 31:407–416.
12. Sivak DA, Crooks GE (2016) Thermodynamic geometry of minimum-dissipation driven barrier crossing. *Phys Rev E* 94:052106.
13. Schmiedl T, Seifert U (2007) Optimal finite-time processes in stochastic thermodynamics. *Phys Rev Lett* 98:108301.
14. Aurell E, Mejía-Monasterio C, Muratore-Ginanneschi P (2011) Optimal protocols and optimal transport in stochastic thermodynamics. *Phys Rev Lett* 106:250601.
15. Manosas M, Ritort F (2005) Thermodynamic and kinetic aspects of RNA pulling experiments. *Biophys J* 88:3224–3242.
16. Nakanishi-Matsui M, et al. (2007) Rotational catalysis of Escherichia coli ATP synthase F1 sector. Stochastic fluctuation and a key domain of the β subunit. *J Biol Chem* 282: 20698–20704.
17. Isralewitz B, Gao M, Schulten K (2001) Steered molecular dynamics and mechanical functions of proteins. *Curr Opin Struct Biol* 11:224–230.
18. Gore J, Ritort F, Bustamante C (2003) Bias and error in estimates of equilibrium free-energy differences from nonequilibrium measurements. *Proc Natl Acad Sci USA* 100: 12564–12569.
19. Liu S, et al. (2014) A viral packaging motor varies its DNA rotation and step size to preserve subunit coordination as the capsid fills. *Cell* 157:702–713.
20. Chen J, et al. (2015) Coupling of mRNA structure rearrangement to ribosome movement during bypassing of non-coding regions. *Cell* 163:1267–1280.
21. Yasuda R, Noji H, Kinosita K, Jr, Yoshida M (1998) F1-ATPase is a highly efficient molecular motor that rotates with discrete 120 degree steps. *Cell* 93:1117–1124.
22. Itoh H, et al. (2004) Mechanically driven ATP synthesis by F1-ATPase. *Nature* 427: 465–468.
23. Rondelez Y, et al. (2005) Highly coupled ATP synthesis by F1-ATPase single molecules. *Nature* 433:773–777.
24. Large SJ, Chetrite R, Sivak DA (2018) Stochastic control in microscopic nonequilibrium systems. *EPL* 124:20001.
25. Bustamante C, Chemla YR, Moffitt JR (2009) High-resolution dual-trap optical tweezers with differential detection: Instrument design. *Cold Spring Harb Protoc* 2009: ip73.
26. Bustamante C, Chemla YR, Moffitt JR (2009) High-resolution dual-trap optical tweezers with differential detection: Data collection and instrument calibration. *Cold Spring Harb Protoc* 2009:ip74.
27. Li PTX, Bustamante C, Tinoco I, Jr (2007) Real-time control of the energy landscape by force directs the folding of RNA molecules. *Proc Natl Acad Sci USA* 104:7039–7044.
28. Hernández Candia CN, Tafoya Martínez S, Gutiérrez-Medina B (2013) A minimal optical trapping and imaging microscopy system. *PLoS One* 8:e57383.
29. Wasserman L (2013) *All of Statistics: A Concise Course in Statistical Inference* (Springer, New York).
30. Akaike H (1974) A new look at the statistical model identification. *IEEE Trans Automat Contr* 19:716–723.